Coulomb explosion effect and the maximum energy of protons accelerated by high-power lasers

E. Fourkal, I. Velchev, and C.-M. Ma
Department of Radiation Physics, Fox Chase Cancer Center, 7701 Burholme Avenue, Philadelphia, Pennsylvania 19111, USA
(Received 17 August 2004; revised manuscript received 12 January 2005; published 25 March 2005)

The acceleration of light ions (protons) through the interaction of a high-power laser pulse with a double-layer target is theoretically studied by means of two-dimensional particle-in-cell simulations and a one-dimensional analytical model. It is shown that the maximum energy acquired by the accelerated light ions (protons) depends on the physical characteristics of a heavy-ion layer (electron-ion mass ratio and effective charge state of the ions). In our theoretical model, the hydrodynamic equations for both electron and heavy-ion species are solved and the test-particle approximation for the light ions (protons) is applied. The heavy-ion motion is found to modify the longitudinal electric field distribution, thus changing the acceleration conditions for the protons.

DOI: 10.1103/PhysRevE.71.036412 PACS number(s): 52.38.Kd, 52.38.Ph

I. INTRODUCTION

The problem of the interaction of ultrahigh-intensity laser pulses with plasmas has attracted considerable interest due to its promising applications in a variety of areas such as the generation of hard x rays, neutrons, electrons, and high-energy ions. The laser-accelerated ion beams have specific characteristics, such as high collimation and high particle flux, which make them very attractive for possible applications in controlled nuclear fusion [1,2], material science [3], the production of short-lived isotopes for medical diagnostics [4], and hadron therapy [5,6].

Many previous experimental studies [7–9] have been directed toward the understanding of different mechanisms of fast proton-ion generation during the interaction of ultrahigh-intensity laser pulses with thin solid structures. Metallic as well as insulator targets were used with a thickness ranging from a few μm to more than 100 μm. The origin of the observed ions and the mechanism of their acceleration still remain matters of debate. The ions are either created and accelerated at the front surface directly illuminated by the incident laser [7] or at the rear surface, where acceleration occurs through the electrostatic field, generated by the space-charge separation [10,11]. It is likely that the particular experimental conditions (the influence of the laser pedestal and the target properties) will determine the acceleration scheme, although in some experiments [9,12] it has been unequivocally shown that proton acceleration occurs at the back surface of the target.

The initially proposed theoretical model for ion acceleration at the back surface of the target heavily relied on the notion of quasineutral plasma expansion into vaccum [13,14]. In this model the accelerating electric field is generated due to space-charge separation in a narrow layer at the front of the expanding plasma cloud, which is assumed to be neutral. In the interaction of ultrashort and ultraintense laser pulses with a solid structure, the assumption of quasineutrality must be abandoned. The results of computer simulations [15,16] suggest that the interaction of petawatt laser pulses with plasma foils leads to the formation of extended regions where plasma quasineutrality is violated, a factor that has to be taken into account when considering ion acceleration by ultraintense pulses. In Ref. [17] the authors described the electric field structure created by two populations of electrons, each following a Boltzmann distribution with different thermal energies. The effects of charge separation have been taken into account by solving Poisson equations (with two-temperature electron components) for the electrostatic potential distribution inside the foil (where ions are present) and outside of it (where only electrons reside). The limitation of this approach lies in the fact that it inherently provides a time-independent description, whereas for a quantitative estimation of ion energies knowledge of the temporal evolution of the electric field profile is required. In this respect the treatment suggested in Ref. [18] offers a possibility for obtaining the spatiotemporal evolution of the self-consistent electrostatic field, leading to an estimation of the maximum energy that ions can acquire in the field.

There are several examples of efficient proton-ion acceleration under the condition of strong charge separation. One of them is the Coulomb explosion of an ion cluster [19]. A laser pulse interacting with the target expels electrons, thus creating a strong electric field inside the foil, which plays a key role in the ion acceleration process. In other cases [20], protons are accelerated by the electric field (time independent) of the ionized target and their dynamics can be described by using the test-particle approximation approach. The multilayer target system and, more specifically, the two-layer one are perfect examples of this particular acceleration scheme. In this structure the first layer consists of heavy ions of mass m_i and specific ionization state Z_i and the second layer (attached to its back surface) consists of ionized hydrogen. Under the action of the laser ponderomotive force, electrons escape from the target, leaving behind a charged layer of heavy ions. If the ion mass is much larger than that of the proton, the dynamics of the ion cluster (Coulomb explosion) is usually neglected during the effective acceleration time of protons. During this time period, the electric field of the ion cluster is considered to be time independent and one is left with the problem of proton acceleration in a stationary, but spatially inhomogeneous electric field.

In reality, however, the proton acceleration time is relatively long ($t \sim 100/\omega_{pe}$) and the influence of both the self-consistent electron dynamics and the ion cluster explosion

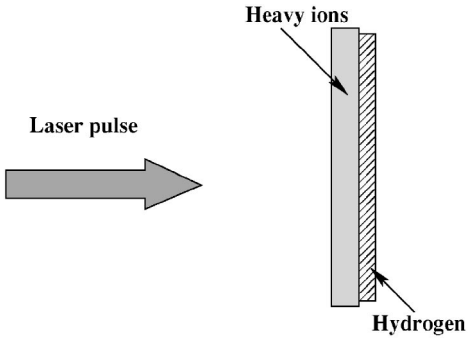

FIG. 1. Schematic diagram of the laser-target system. The target consists of a high-density heavy-ion slab with a low-density hydrogen layer attached to its back surface.

renders the electric field time dependent. As a result, the maximum proton energy becomes a function of the physical properties of the cluster (e.g., ion mass, charge state).

In this paper, we investigate the influence of the cluster's characteristics on the accelerating electric field and the maximum proton energy using particle-in-cell (PIC) simulations of laser interaction with a double-layer target. In Sec. III, we present a theoretical model of electric field evolution that accounts for the influence of the Coulomb explosion effect. The model is based on a solution of one-dimensional (1D) hydrodynamic equations for electron and ion components. The results obtained within the realm of this model explain the correlation between the physical parameters of the heavy-ion layer on the one hand and the structure of the electric field and maximum proton energy on the other.

II. RESULTS OF COMPUTER SIMULATIONS

A 2D PIC numerical simulation code [21,22] was used to describe the interaction of a high-power laser pulse with a double-layer target. The PIC simulation is an indispensable tool allowing the characteristic features of laser interactions with plasmas to be revealed, specifically in cases where the contribution of nonlinear and kinetic effects makes the multidimensional analytical approach extremely difficult. In this paper we consider the acceleration of protons in the interaction of a laser pulse with a double-layer target. The calculations were performed in a 2048×512 simulation box with grid size $\Delta=0.04$ μm and total number of simulated quasiparticles 4×10^6. Periodic boundary conditions for particles and electromagnetic fields have been used. In order to minimize the influence of the boundary conditions on the outcome of the simulations the maximum simulation time was set to $80/\omega_{pe}\approx225$ fs, where ω_{pe} is the electron plasma frequency averaged over the simulation box. Several types of targets with different electron-to-ion mass ratios and ionization states have been investigated. It is worth noting that the ionization state of ions should be calculated from the solution to the wave equation for a given multielectron system in the presence of an ultrahigh-intensity laser pulse, a difficult task for any system with two or more electrons [23]. Therefore, the ion charge state is considered to be a parameter rather than a calculated value in this work.

Figure 1 shows the schematic diagram of the double-layer target. The system consists of 0.4-μm-thick high-density ($n_e\simeq6.4\times10^{22}$ cm^{-3}) heavy-ion foil with a 0.16-μm-thick low-density ($n_e\simeq2.8\times10^{20}$ cm^{-3}) hydrogen layer attached to its back surface. The target was positioned in the middle of the simulation box with the laser pulse entering the interaction region from the left. The electric field of the laser pulse is polarized along the y axis with a dimensionless amplitude $a=eE_0/m_e\omega c=30$, which corresponds to a laser peak intensity of 1.9×10^{21} W/cm^2 for a laser wavelength of $\lambda=0.8$ μm. The laser pulse was Gaussian in shape with length (duration) and width (beam diameter) of 15λ and 8λ [full width at half maximum (FWHM)], respectively, which corresponds to approximately a 890-TW system.

In Fig. 2 the spatial distribution of E_x (longitudinal) and E_y (transverse) components of the electric field is presented at $t=40/\omega_{pe}$. Even though the target thickness is much larger than the collisionless skin depth $\delta=c/\omega_{pe}$, the incident pulse splits into reflected and transmitted components due to the relativistic decrease of the electron plasma frequency [24]. As a result, a part of the laser energy goes through the overcritical density target. The longitudinal electric field, which accelerates protons, extends over large spatial distances on both sides of the target. This field is created by the expanding electron cloud accelerated in the forward and backward directions by the propagating laser pulse. Figure 3 shows the energy distributions of (a) electrons, (b) protons, and (c) heavy ions at $t=32/\omega_{pe}$ for different values of the structural parameter of the substrate, $\chi=Z_im_e/m_i$. It can be seen that the electron and heavy-ion energy spectra resemble a quasithermal distribution whereas the proton energy spectrum has a quasimonoenergetic shape with a characteristic energy depending on the value of χ. In Ref. [25] it is shown that in a double-layer target geometry a high-quality proton beam can indeed be generated. When a laser pulse interacts with the target, both the heavy atoms in the first layer and the hydrogen atoms in the second are ionized; a plasma sandwich structure is thus created, consisting of the high-Z heavy-ion plasma and the ionized hydrogen "attached" to its back surface. Under the action of the ponderomotive force, some electrons are expelled from the plasma (in the forward and backward directions), thus producing a longitudinal electric field that accelerates the thin layer of protons. If the number of protons in this layer is sufficiently small, the longitudinal electric field is not significantly perturbed. Under this condition the protons are accelerated by the electric field created between the charged heavy-ion layer and the fast electron cloud [20]. In this case a thinner proton layer results in a narrower energy spread of the accelerated protons. This is due to the fact that at any given time the protons in a narrow slab experience almost the same accelerating electric field. This peculiarity in the proton dynamics can also be seen from the spatial distributions of the particles shown in Fig. 4 for (a) electron, (b) proton, and platinum-ion ($Z_i=4, m_i/m_p=195$) densities in the (x,y) plane. At time $t=32/\omega_{pe}$ the proton layer is already detached from the high-Z target and travels almost undistorted in a forward direction. At the same time, the heavy-ion layer is expanding at a much slower rate due to its greater mass. The characteristic response time of ions is on the order of ion plasma frequency

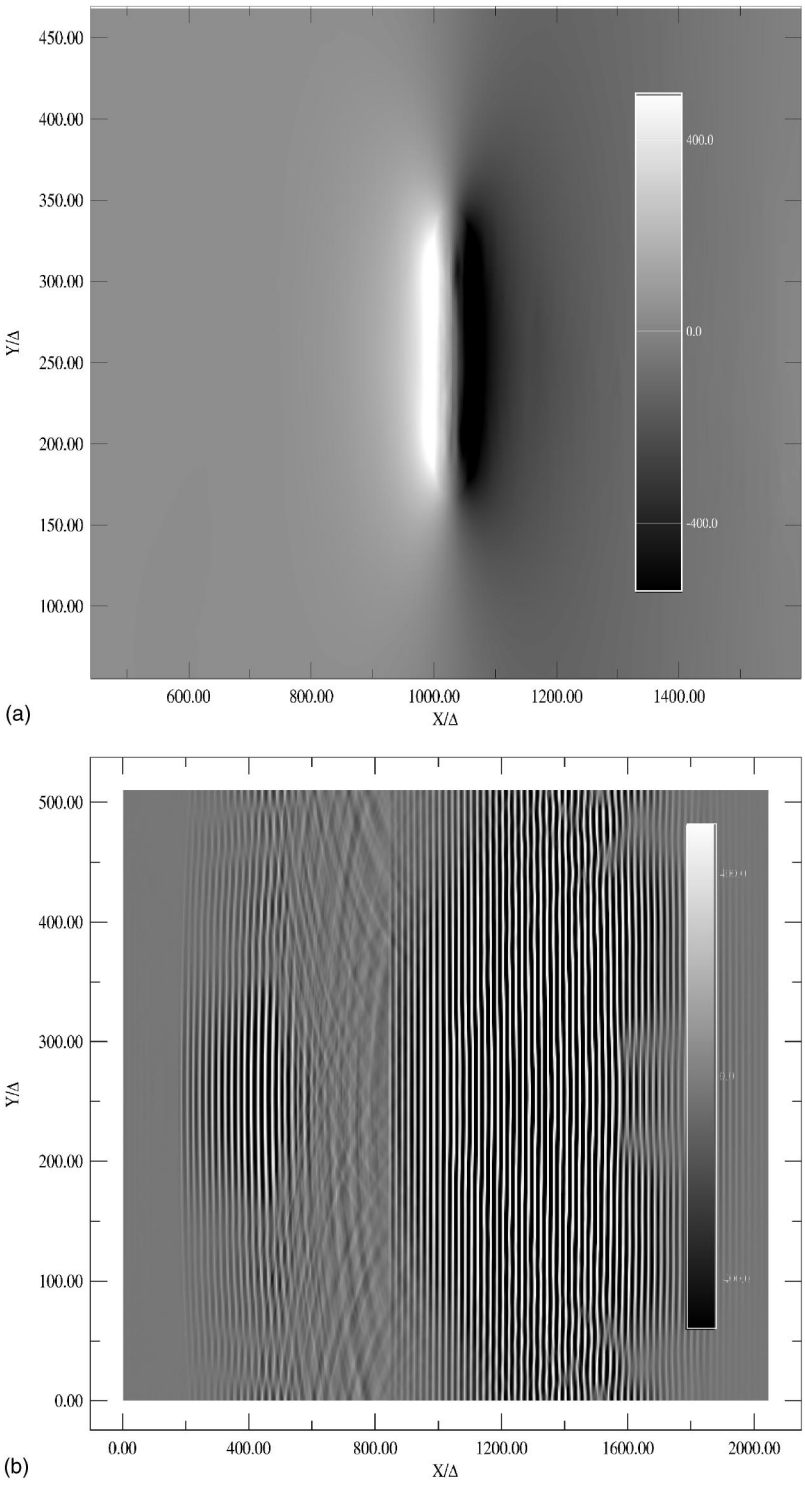

FIG. 2. Distribution of (a) the longitudinal (E_x) and (b) the transverse (E_y) components of the electric field in the (x,y) plane at $t=40/\omega_{pe}$. The target is initially located at $x/\Delta=1025$. $\omega_{pe}\approx 3.57\times 10^{14}$ s^{-1}, and $\Delta=4\times 10^{-8}$ m.

$1/\omega_{pi}=\sqrt{m_i/4\pi e^2 n_0 Z_i^2}$, where n_0 is the ion density. Once the electrons have left the target, the ion layer begins to expand under the action of the Coulomb repulsive forces. Even though the ion response time is longer than that of protons, its dynamics will inevitably influence the longitudinal electric field, thus affecting the acceleration of the proton beam. As one can see from Fig. 3 a larger value of the parameter $\chi=Z_i m_e/m_i$ results in a more effective proton acceleration (a nearly 50% increase for carbon substrate compared to the platinum one, assuming the same ionization state $Z_i=4$). In other words, a more robust ion expansion leads to a more efficient proton acceleration. At first, this result seems somewhat counterintuitive since ion expansion is accompanied by a reduction of the longitudinal electric field (that electric field energy partly transforms into the kinetic energy of the expanding ions) and should presumably lead to lower proton energies. A simple estimation of the maximum proton energy can be ascertained from the picture suggested in Ref. [20] where the longitudinal electric field of the charged layer of heavy ions is approximated by that created by a charged

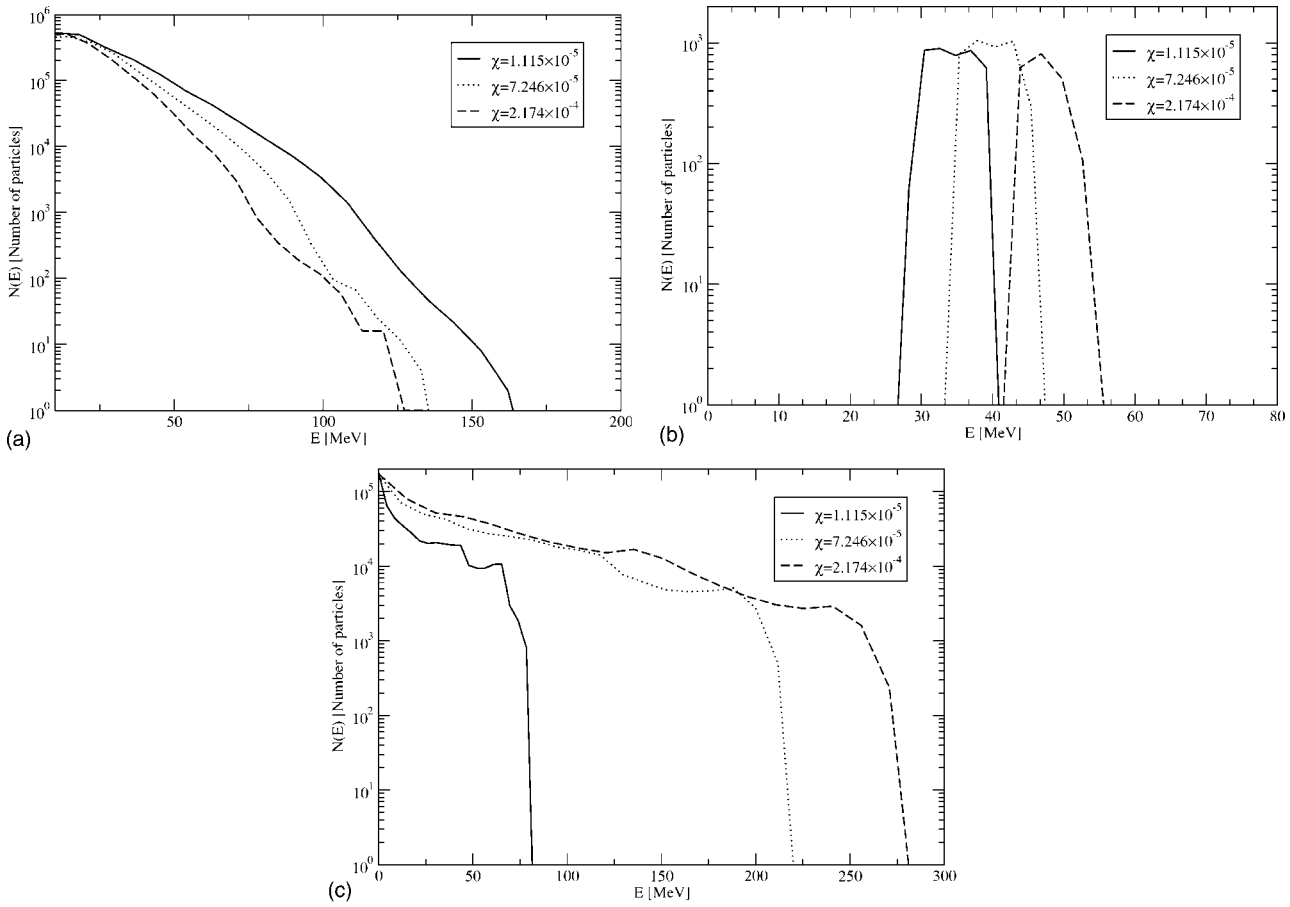

FIG. 3. Energy distributions of (a) electrons, (b) protons, and (c) heavy ions at $t=32/\omega_{pe}$ for three different values of the structural parameter χ. $\omega_{pe}\approx 3.57\times 10^{14}\ \mathrm{s}^{-1}$.

ellipsoid with its major semiaxis equal to the transverse dimension of the target R_0 and its minor semiaxis equal to l ($2l$ is the thickness of a target). In this case the longitudinal electric field and the electrostatic potential have the forms [26]

$$E_x(x)=\frac{8\pi e n_0 Z_i l R_0^2}{3}\frac{1}{(R_0^2-l^2+x^2)}, \tag{1}$$

$$\phi(x)=\frac{4\pi e n_0 Z_i l R_0^2}{3\sqrt{R_0^2-l^2}}\arctan\left[\frac{\sqrt{R_0^2-l^2}}{x}\right]. \tag{2}$$

The maximum kinetic energy that a proton acquires in this field equals its potential energy at the surface of the target. Under the assumption that the target thickness is much less than its transverse dimension one obtains

$$\mathcal{E}\approx 2\pi Z_i e^2 n_0 l R_0. \tag{3}$$

This estimation gives an upper limit to the maximum proton energy, which can be attained under the assumption that all electrons escape from the target, acquiring enough kinetic energy to overcome the attractive electric field (so that they never return to the target). In reality, however (for laser intensity used in our simulations), only a small fraction of electrons escape the target. The rest remain in the vicinity of the target with some of them performing a rather complicated oscillatory motion (see next section). This effect greatly reduces the total charge density in the foil, thus substantially lowering the maximum proton energy estimated by Eq. (3). Naturally, Eq. (3) can not explain the dependence of the proton energy on the ion mass and ionization state of the foil (for a given initial electron density). The combination of both the Coulomb explosion of the target and the electron dynamics in a self-consistent electric field renders the field time dependent in contrast with the simplified model offered by Eq. (1). Logically, the dependence of the maximum proton energy on the target parameters can only come from the influence of the ion motion on the longitudinal electric field. Figure 5 shows the electric field profile as a function of the distance from the target in the longitudinal direction (that direction of proton acceleration) at $t=32/\omega_{pe}$ for three different ion-to-proton mass ratios, but otherwise the same ionization state of $Z_i=4$. As one can see the electric field structure is such that its magnitude at the surface of the expanding heavy-ion layer (the point where the electric field starts decreasing with distance) increases with the ion mass (because of the less efficient conversion of the field energy into the kinetic energy of ions). On the other hand, farther away from the target the electric field exhibits an opposite trend in which its value decreases with increasing ion-to-proton mass ratio. Since a layer of protons quickly leaves the surface of

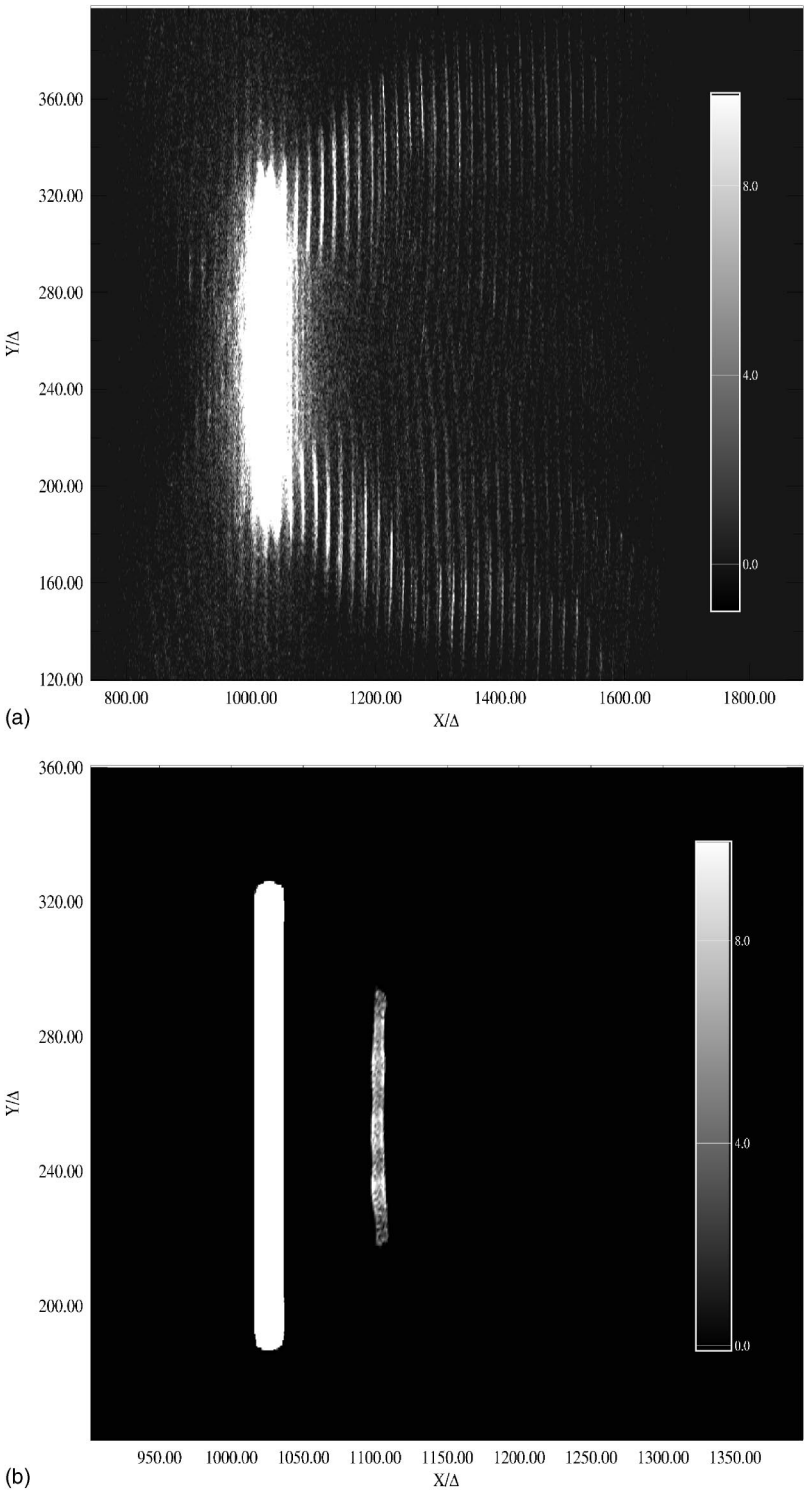

FIG. 4. Spatial distributions of the (a) electron, (b) proton, and platinum-ion densities in the (x,y) plane at $t=32/\omega_{pe}$. The target is initially located at $x/\Delta=1025$. $\omega_{pe}\approx 3.57\times 10^{14}$ s^{-1}, and $\Delta=4\times 10^{-8}$ m.

the target (before any significant target expansion occurs), the field distribution beyond the foil will ultimately determine the maximum proton energy.

III. FORMULATION OF THE PROBLEM

Let us consider the problem of proton acceleration in the self-consistent electric field created by the expanding electron and heavy-ion clouds. Our specific goal is to evaluate the influence of the Coulomb explosion effect on the structure of the accelerating electric field. Since the interaction of a high-intensity laser pulse with plasma constitutes an extremely complicated physical phenomenon, we will consider a somewhat simplified physical picture that could allow us to clarify certain aspects related to the evolution of the longitudinal electric field.

We assume that electrons are initially located inside the target with a flat density distribution $n_e=Z_i n_0\theta(l/2-|x|)$,

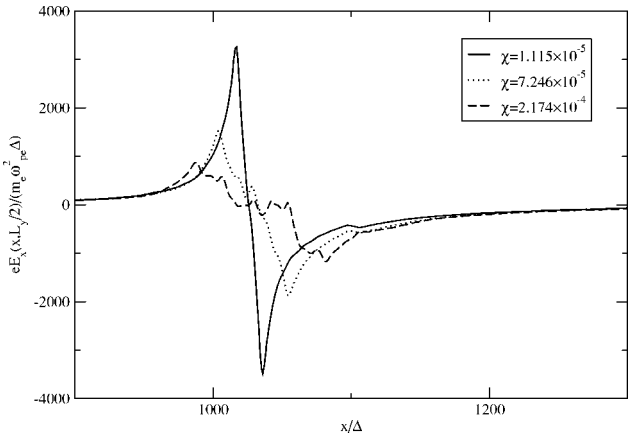

FIG. 5. Longitudinal electric field profile $E_x(x,L_y/2)$ as a function of x at $t=32/\omega_{pe}$ for three different ion-to-proton mass ratios and the same ionization state $Z_i=4$. $\omega_{pe}\approx 3.57\times 10^{14}$ s^{-1} and $\Delta=4\times 10^{-8}$ m.

where $n_{e,0}=Z_i n_0$ and $\theta(x)$ is the Heaviside unit-step function. Under the action of a high-intensity short laser pulse, the electrons gain longitudinal relativistic momentum $p_{e,0}$. This momentum in general is a function of the initial electron position $x_i(0)$. For the sake of simplicity we assume a model, in which half of the electrons (located in the interval $0<x<l/2$) gains momentum $p_{e,0}$ from the laser pulse and the other half (located in the interval $-l/2<x<0$) gains negative momentum $-p_{e,0}$. This model is somewhat descriptive of the electron fluid motion due to its interaction with the laser pulse where the forward-moving particles correspond to those that are accelerated by the ponderomotive force, while the backward-moving electrons are extracted in the opposite direction due to the process known as "vacuum heating" [27,28]. This assumption constitutes a considerable simplification in the description of the initial electron fluid momentum distribution. Nonetheless, it should properly describe the relevant physical mechanisms of electric field evolution.

A. Self-consistent evolution of electron cloud

The expansion of plasma into the vacuum can be described by using one-dimensional hydrodynamic equations for electron and ion components. As mentioned earlier, it is assumed that the proton layer does not perturb the generated electric field. In this case the equations of hydrodynamics for both components are

$$\frac{\partial n_e}{\partial t}+\frac{\partial (n_e v_e)}{\partial x}=0, \tag{4a}$$

$$\frac{\partial p_e}{\partial t}+v_e\frac{\partial p_e}{\partial x}=-eE(x,t), \tag{4b}$$

$$\frac{\partial n_i}{\partial t}+\frac{\partial (n_i v_i)}{\partial x}=0, \tag{4c}$$

$$\frac{\partial v_i}{\partial t}+v_i\frac{\partial v_i}{\partial x}=\frac{Z_i e}{m_i}E(x,t), \tag{4d}$$

$$\frac{\partial E}{\partial x}=4\pi e[Z_i n_i(x,t)-n_e(x,t)], \tag{4e}$$

where n_e and n_i are the electron and ion densities and v_e and p_e are the electron velocity and momentum related through the expression $v_e=cp_e/(m_e^2c^2+p_e^2)^{1/2}$. In Eq. (4d) we assume nonrelativistic ion kinematics during the course of the Coulomb explosion.

In order to solve Eqs. (4) we switch from the Euler variables (x,t) to those of the Lagrange (x_0,t) [29], where x_0 is the electron fluid element coordinate at $t=0$. Both sets of coordinates are related through the following expression:

$$x(x_0,t)=x_0+\xi_e(x_0,t), \tag{5}$$

where $\xi_e(x_0,t)$ is the displacement of the electron fluid element from its initial position x_0 at time t. In the new variables Eqs. (4) read

$$\tilde{n}_e(x_0,t)=n_e(x,t)=\tilde{n}_e(x_0,0)\frac{\partial x_0}{\partial x}, \tag{6a}$$

$$\frac{\partial \tilde{p}_e(x_0,t)}{\partial t}=-e\tilde{E}(x_0,t), \tag{6b}$$

$$\frac{\partial \tilde{n}_i}{\partial t}-v_e\frac{\partial x_0}{\partial x}\frac{\partial \tilde{n}_i}{\partial x_0}+\frac{\partial (\tilde{n}_i v_i)}{\partial x_0}\frac{\partial x_0}{\partial x}=0, \tag{6c}$$

$$\frac{\partial v_i}{\partial t}-(v_e-v_i)\frac{\partial v_i}{\partial x_0}\frac{\partial x_0}{\partial x}=\frac{Z_i e}{m_i}\tilde{E}(x_0,t), \tag{6d}$$

$$\frac{\partial \tilde{E}}{\partial x_0}\frac{\partial x_0}{\partial x}=4\pi e\left(Z_i\tilde{n}_i(x_0,t)-\tilde{n}_e(x_0,0)\frac{\partial x_0}{\partial x}\right), \tag{6e}$$

where the tilde is used to designate functions in the new variables (x_0,t); $v_e=\partial\xi_e/\partial t$ and v_i are the electron and ion fluid velocities, and $\tilde{n}_e(x_0,0)=n_e(x,0)$ is the initial electron density. As one can see, the form of the hydrodynamic equations for the electron fluid component is greatly simplified in the new variables, whereas the equations for the ions are somewhat more complex compared to those expressed through variables (x,t). Because of the smallness parameter $\chi=Z_i m_e/m_i\ll 1$, the ion motion in Eqs. (6) is considered a perturbation to the zeroth-order solution, which corresponds to the case of motionless ions. The solution to Eqs. (6) with $v_i=0$ and $\tilde{n}_i(x_0,t)=n(x,0)=n_0\theta(l/2-|x|)$ was obtained in Ref. [18] and for the case of constant initial electron momentum distribution are given by the expressions

$$\tilde{E}(x_0,t)=-4\pi eZ_i n_0\begin{cases}\dfrac{l}{2}-x_0, & \dfrac{l}{2}<x_0+\xi_e,\\ \xi_e(x_0,t), & |x_0+\xi_e|<\dfrac{l}{2},\\ -\dfrac{l}{2}-x_0, & x_0+\xi_e<-\dfrac{l}{2},\end{cases} \tag{7}$$

$$p_e(x_0,t) \approx \begin{cases} p_{e,0}\cos\left(\dfrac{\omega_{pe}t}{\Gamma}\right), & t \le \tau^*, 0 < x_0 + \xi_e < \dfrac{l}{2}, \\ p_{e,0}\cos\left(\dfrac{\left(\dfrac{l}{2}-x_0\right)\omega_{pe}}{v_{e,0}\Gamma}\right) + \dfrac{\kappa(x_0)}{v_{e,0}}\left(\dfrac{l}{2}-x_0-v_{e,0}t\right), & t > \tau^*, x_0 + \xi_e > \dfrac{l}{2}, \end{cases} \tag{8a}$$

$$\xi_e(x_0,t) \approx \begin{cases} \Gamma\dfrac{c}{\omega_{pe}}\arctan\left[\dfrac{p_{e,0}\sin\left(\dfrac{\omega_{pe}t}{\Gamma}\right)}{\sqrt{m_e^2c^2+p_{e,0}^2\cos^2\left(\dfrac{\omega_{pe}t}{\Gamma}\right)}}\right], & t \le \tau^*, \\ \left(\dfrac{l}{2}-x_0\right) + \dfrac{c}{\kappa(x_0)}\left(\sqrt{m_e^2c^2+p_{e,0}^2\cos^2\left(\dfrac{\left(\dfrac{l}{2}-x_0\right)\omega_{pe}}{v_{e,0}\gamma}\right)}\right. \\ \left. -\sqrt{m_e^2c^2+\left[p_{e,0}\cos\left(\dfrac{\left(\dfrac{l}{2}-x_0\right)\omega_{pe}}{v_{e,0}\gamma}\right)+\dfrac{\kappa(x_0)}{v_{e,0}}\left(\dfrac{l}{2}-x_0-v_{e,0}t\right)\right]^2}\right), & t > \tau^*, \end{cases} \tag{8b}$$

$$\kappa(x_0) = 4\pi Z_i e^2 n_0\left(\frac{l}{2}-x_0\right),$$

where $\tau^* \approx (l/2-x_0)/v_{e,0}(v_{e,0}\approx c)$ is the transit time during which electrons are inside the target $(0<x<l/2)$ and $\Gamma(p_{e,0})$ is a parameter that depends only on the initial electron momentum $p_{e,0}$. Its value is found from the numerical solution of Eq. (6b) for the case when electrons are inside the target and its simple analytical form $\Gamma(p_{e,0})=[1+a(p_{e,0}/m_ec)^2]^b$ is shown in Fig. 6. Equations (8) describe only the electrons that satisfy the following condition:

$$\Gamma(p_{e,0})\frac{c}{\omega_{pe}}\arctan\left[\frac{p_{e,0}}{m_ec}\right] > \frac{l}{2}-x_0,$$

which ensures that an electron reaches the boundary of the target (some electrons that are initially located deeply inside the target may not reach its surface). It should be noted here that Eqs. (8a) and (8b) are somewhat different from those published in Ref. [18] due to accounting for the finite time required for electrons to leave the target. As one can see, at time

$$t_{max} = \frac{p_{e,0}}{\kappa(x_0)}\cos\left[\frac{\left(\dfrac{l}{2}-x_0\right)\omega_{pe}}{v_{e,0}\Gamma}\right] + \frac{\dfrac{l}{2}-x_0}{v_{e,0}},$$

the electron fluid displacement reaches the maximum value

$$\xi_{max} = \left(\frac{l}{2}-x_0\right) + \frac{c}{\kappa(x_0)} \times \left\{\sqrt{m_e^2c^2+p_{e,0}^2\cos^2\left[\frac{\left(\dfrac{l}{2}-x_0\right)\omega_{pe}}{v_{e,0}\Gamma}\right]} - m_ec\right\}$$

and decreases afterwards. Eventually the electron fluid element returns to the target and reappears on the other side. Thus the general dynamics of the electron component can be described as an oscillatory motion around the target. The return time or the period of oscillations depends on the initial position x_0 of the fluid element. Electrons that initially are closer to the boundary of the plasma slab $[(l/2-x_0)\to 0]$ have longer return times. The presence of this asynchronicity in the electron fluid motion quickly leads to a "mixing" of the initially (set by the initial conditions) "ordered" electron trajectories. After a few tens of plasma period cycles the electron phase space and density distributions evolve in such a way that the majority of electrons are localized around the

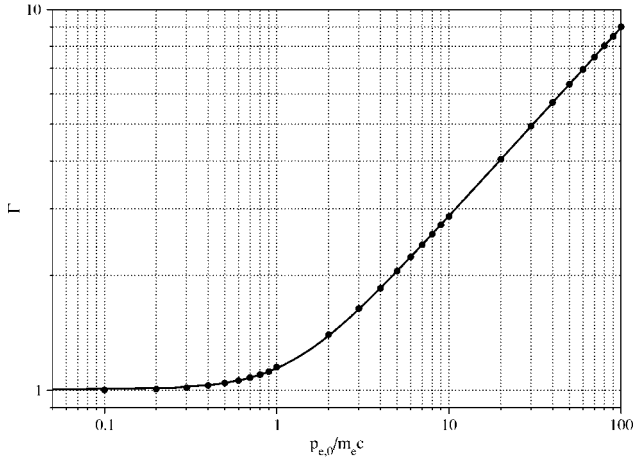

FIG. 6. The numerically obtained parameter Γ approximated by the simple expression $\Gamma(\tilde{p}_e,0)=(1+a\tilde{p}_{e,0}^2)^b$, where $a=0.691(4)$, $b=0.2481(2)$, and $\tilde{p}_{e,0}$ is the normalized electron initial momentum.

target, considerably shielding its charge. Figure 7 shows the phase-space (a) and density (b) distributions of electrons at time $t=150/\omega_{pe}$ obtained from 1D PIC simulations. As mentioned earlier, the initial condition for the electron momentum distribution was $p_{e,0}(x)=\mathrm{sgn}(x)\theta(l/2-|x|)10m_e c$. Figure 7(a) also shows the 1D PIC simulation results of the electron phase-space distribution for the case when laser dynamics is included. As one can see, the "idealized" model of the initial electron momentum distribution adopted in this work leads to almost the same final electron phase-space distribution as that calculated with the laser pulse present. The late-time phase-space distribution clearly shows the formation of an electron cloud concentric with the expanding ion layer having a rather broad momentum distribution. One can also see an electron structure at a distance from the target propagating away from it with velocity nearly equal to $v_{e,0}$. These are the particles that have originated at a front of the electron cloud ($|x_0|\to l/2$).

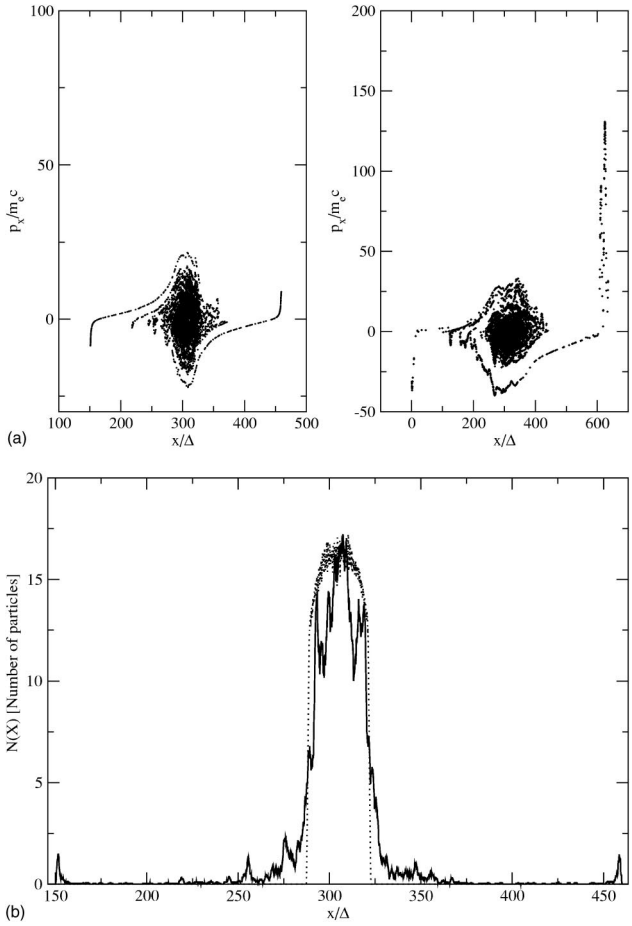

FIG. 7. Electron phase-space spectrum (a) for the "idealized" initial electron momentum distribution (left) at $t=150/\omega_{pe}$ and that calculated with the laser pulse present (right) at $t=300/\omega_{pe}$; density distributions (b) for electrons (solid line) and ions (dotted line) at $t=150/\omega_{pe}$. The initial electron momentum distribution $p_{e,0}=10m_e c$ for $(0<x<l/2)$ and $p_{e,0}=-10m_e c$ for $(-l/2<x<0)$. $\omega_{pe}=4\times10^{14}$ s^{-1} and $\Delta=7.5\times10^{-7}$ m.

B. Coulomb explosion and the electric field structure beyond the target's surface

The Coulomb explosion of the target, which leads to the gradual expansion of the ion layer, renders the ion density time dependent. According to Eq. (4e), the change in ion density will inevitably influence the longitudinal electric field profile. The electric field distribution [see Eq. (7)] calculated in the previous section assumes an infinite ion mass ($\chi=0$). Therefore, in order to find out how the field structure changes with the expanding ion layer, one needs to obtain the spatial and temporal evolution of ion density. Its development is governed by the action of the electric field inside the target. Under the assumption that the electrons have left the target, the self-consistent ion evolution can be found from the solution to the 1D ion hydrodynamic equations. As in the previous section, it is advantageous to work in a Lagrange representation, where the connection between both coordinates is expressed through the ion fluid element displacement:

$$x(x_0,t)=x_0+\xi_i(x_0,t). \tag{9}$$

The ion hydrodynamic equations in the Lagrange coordinates have the following form:

$$\tilde{n}_i(x_0,t)=n_i(x,t)=\tilde{n}_i(x_0,0)\frac{\partial x_0}{\partial x}, \tag{10a}$$

$$\frac{\partial^2\xi_i(x_0,t)}{\partial t^2}=\frac{Z_i e}{m_i}\tilde{E}_{in}(x_0,t), \tag{10b}$$

$$\frac{\partial\tilde{E}_{in}}{\partial x_0}=4\pi eZ_i\tilde{n}_i(x_0,0), \tag{10c}$$

where E_{in} denotes the electric field inside the target. For a flat initial density distribution $\tilde{n}_i(x_0,0)=n_0\theta(l/2-|x_0|)$, the solution of Eqs. (10) has the form

$$\tilde{E}_{in}(x_0,t)=4\pi en_0Z_i x_0, \tag{11a}$$

$$\xi_i(x_0,t) = \chi\frac{\omega_{pe}^2}{2}t^2x_0. \tag{11b}$$

As seen from Eq. (11a), the electric field vanishes in the middle of the target and linearly increases (in absolute value) away from it. Using Eq. (11b) and relation (9) one can express the electric field and the ion density through the Euler variables (x,t) to give

$$n_i(x,t) = \frac{n_0}{1+\frac{\chi\omega_{pe}^2t^2}{2}}\theta\left(\frac{l}{2}-\frac{|x|}{1+\frac{\chi\omega_{pe}^2t^2}{2}}\right), \tag{12a}$$

$$E_{in}(x,t) = \frac{4\pi Z_i e n_0 x}{1+\frac{\chi\omega_{pe}^2t^2}{2}}, \quad |x| \leqslant \frac{l}{2}\left(1+\frac{\chi\omega_{pe}^2t^2}{2}\right), \tag{12b}$$

$$E_{out}(x,t) = \pm 4\pi Z_i e n_0\frac{l}{2}, \quad |x| > \frac{l}{2}\left(1+\frac{\chi\omega_{pe}^2t^2}{2}\right). \tag{12c}$$

Equation (12a) describes the evolution of 1D ion slabs under the action of the Coulomb repulsive force (Coulomb explosion).

As mentioned earlier, the simulation results suggest that the maximum kinetic energy of the accelerated protons is determined by the structure of the longitudinal field beyond the surface of the target. Therefore we are interested in the spatio temporal evolution of the electric field near the front of the expanding electron cloud. The initial conditions for these electrons are $x_0 \to l/2$ and their displacement $\xi_e(x_0,t)$ for $l/2 < x_0+\xi_e(x_0,t)$ takes the form

$$\xi_e(x_0,t) \approx v_{e,0}t - \frac{\omega_{pe}^2t^2}{2\left(1+\frac{p_{e,0}^2}{m_e^2c^2}\right)^{3/2}}\left(\frac{l}{2}-x_0\right). \tag{13}$$

Equation (13) was obtained from the solution, Eq. (8b), in the limit $l/2-x_0 \to 0$ and together with the definition (5) constitutes the inversion procedure, which allows one to go back to Euler coordinates (x,t) and determine the electric field structure (in x,t coordinates) at the front of the electron cloud as presented in Ref. [18]. The calculated field distribution, however, does not reflect the influence of the ion motion. In order to obtain the contribution of ions, one has to go on to the next order in the expansion of the electric field in the smallness parameter χ by substituting the density distribution function from Eq. (12a) into Eq. (6e):

$$\frac{\partial\tilde{E}}{\partial x_0} = 4\pi e Z_i n_0\left[\frac{1}{1+\frac{\chi\omega_{pe}^2t^2}{2}}\theta\left(\frac{l}{2}-\frac{x_0+\xi_e(x_0,t)}{1+\frac{\chi\omega_{pe}^2t^2}{2}}\right)\left[1+\frac{\partial\xi_e(x_0,t)}{\partial x_0}\right]-\theta\left(\frac{l}{2}-x_0\right)\right], \quad \text{for } \frac{l}{2} < x_0+\xi_e(x_0,t). \tag{14}$$

Using the Lagrange displacement for the electrons given by Eq. (13) we integrate Eq. (14) to arrive at

$$\tilde{E}(x_0,t) = 4\pi Z_i e n_0\left(\frac{l}{2}-x_0-\frac{v_{e,0}t-\frac{l\omega_{pe}^2t^2}{4F}}{1+\frac{\chi\omega_{pe}^2t^2}{2}}+C(t)\right),$$

where $F=(1+p_{e,0}^2/m_e^2c^2)^{3/2}$ and $C(t)$ is an arbitrary function of time appearing as a result of indefinite integration. Its form can be found from the requirement that when $\chi=0$, the electric field has to be equal to that given by Eq. (7). Therefore, the structure of the electric field at the front of electron cloud is

$$\tilde{E}(x_0,t) = 4\pi Z_i e n_0\left(\frac{l}{2}-x_0+\frac{\left(v_{e,0}t-\frac{l\omega_{pe}^2t^2}{4F}\right)\frac{\chi\omega_{pe}^2t^2}{2}}{1+\frac{\chi\omega_{pe}^2t^2}{2}}\right). \tag{15}$$

As one can see, the incorporation of the ion motion into the hydrodynamic description of both components renders the longitudinal electric field (at the front of expanding electron cloud) dependent on the physical parameters of the ions. The dependence is such that a larger value of the parameter χ results in larger electric field; for relativistic electrons, $v_{e,0}t > l\omega_{pe}^2t^2/(4F)$ for $t<\tau\sim 1000/\omega_{pe}$. This increase in the field strength will inevitably lead to higher proton energy, which was also observed in the 2D PIC simulations (see Fig. 3). One must note, however, that Eq. (15) was obtained under the assumption that electrons do not return to the target. As we discussed in the previous section, the majority of electrons will eventually come back, performing complicated oscillatory motion around the slab. The presence of these electrons will shield part of the total charge in the target, reducing its effective charge density. This leads to an overestimation of the contribution of ion motion, but its dependence on the physical characteristics of the target should remain intact.

IV. CONCLUSIONS

Using PIC simulations and a hydrodynamic analytical model, we have investigated the proton acceleration during the interaction of petawatt laser pulses with double-layer targets. The main purpose of this work is to quantitatively understand the role the heavy-ion slab plays in the efficiency of the proton acceleration—more specifically, the influence of the Coulomb explosion effect on the longitudinal electrostatic field. As electrons are expelled from the target, a strong electrostatic field is generated in the region between the target's surface and the front of the expanding electron cloud. The spatial and temporal evolution of this field is determined by both the ion dynamics inside the target (the Coulomb explosion) and the self-consistent electron dynamics outside of it. PIC simulation results suggest that more robust ion expansion leads to more energetic protons. The simulated

longitudinal electric field profile exhibits a trend in which a larger value of a parameter $\chi = Z_i m_e / m_i$ leads to larger values of the electric field in the region beyond the target's surface. This increase in the field strength will ultimately lead to more energetic protons. Up to 50% difference in the maximum proton energy was observed for the carbon substrate versus that made of platinum, but otherwise the same ionization state. With the help of a simplified 1D hydrodynamic model, we obtain the electric field profile at the front of the expanding electron cloud and find that indeed taking into account the ion motion in the hydrodynamic description of electron-ion plasma leads to an increase in the electric field strength in the region beyond the surface of the target. One important point, however, is related to the role of the electrons in the overall evolution of the electric field. If there were no electrons present, the electric field inside the expanding ion target would be lower for substrates with larger values of the structural parameter χ, whereas its magnitude outside the target's surface would be the same, irrespective of the value of χ, as can be seen from Eqs. (12b) and (12c). This would eventually lead to lower energies for the accelerated protons, which contradicts the simulation results as well as the analytical predictions. Thus, the observed increase in the magnitude of the electric field beyond the target's surface is a result of the combined dynamics of both the ion and electron components.

We would also like to briefly touch on the issue of whether theoretically predicted dependence of the final proton energy on the substrate structural parameter has been observed in experimental investigations. There have been a number of experimental studies of proton acceleration by high-power lasers. Plastic as well as metallic (Al, Au) substrates were used. The resulting proton energy differed by not only its maximum value, but also the shape of energy distributions. Different experiments had different target thicknesses, prepulse contrast ratios, and peak laser intensities, making it virtually impossible to unequivocally link the measured proton spectrum to the characteristics of the substrates used in the investigations. Thus, in order to be able to observe the effect described in this paper, one needs to assure that the same laser pulse characteristics and target thicknesses are used.

There are several important issues that are not included in the present analysis. As already mentioned, the ionization state of ions is treated as a parameter, rather than a calculated value. On a qualitative level it is feasible to ascertain that for a given laser intensity, the substrates with larger atomic masses can be ionized to higher ionization states. Whereas in order to quantitatively predict which substrate will maximize the proton energy, one needs a reliable calculation method for the effective atomic ionization state. In this respect the work by Augst *et al.* [23] (carried out for noble gasses only) can be used as a possible starting point to further investigate other elements.

Another issue that has not been taken into account in the simulations is related to the collisional effects. The electron-ion collisions in the presence of laser light lead to inverse bremsstrahlung heating of the electron component, introducing an extra mechanism for absorption of the light. Collisional effects may also be important in the description of normal and anomalous skin effects, thus influencing the fraction of laser light that gets transmitted through the target.

The final point we would like to mention is related to the dimensionality of the considered problem and how it might affect the present results. It is known that 2D PIC simulations are quantitatively different from those in 3D due to the difference in the form of the Coulomb interaction potential between the elementary charges ($\phi \sim \ln r$ in 2D versus $\phi \sim 1/r$ in 3D). One ramification of this salient point lies in a fact that the maximum proton energy predicted by 2D simulations is overestimated compared with the 3D simulation model. Another important question is whether the predicted dependence of the maximum proton energy on the substrate structure parameter χ will be observed in 3D simulations. Since both the 1D theoretical model and 2D simulations predict the existence of this feature, one is led to a conclusion that this effect will be present in 3D modeling, a proof of which is left for our future investigations.

ACKNOWLEDGMENTS

This work is in part supported by NIH (Grant No. CA78331), Strawbridge Family Foundation, and Varian medical systems.

[1] M. Roth, T. Cowan, M. Key, S. Hatchett, C. Brown, W. Fountain, J. Johnson, D. Pennington, and R. Snavely, Phys. Rev. Lett. **86**, 436 (2001).
[2] V. Bychenkov, W. Rozmus, and A. Maksimchuk, Plasma Phys. Rep. **27**, 1017 (2001).
[3] F. Boody, R. Hoepfl, and H. Hora, Laser Part. Beams **14**, 443 (1996).
[4] M. Santala, M. Zepf, F. Beg, E. Clark, A. Dangor, K. Krushelnick, M. Tatarakis, and I. Watts, Appl. Phys. Lett. **78**, 19 (2001).
[5] S. Bulanov and V. Khoroshkov, Plasma Phys. Rep. **28**, 453 (2002).
[6] E. Fourkal, B. Shahine, M. Ding, J. Li, T. Tajima, and C.-M. Ma, Med. Phys. **29**, 2788 (2002).
[7] E. Clark, K. Krushelnick, M. Zepf, F. Berg, M. Tatarakis, A. Machacek, M. Santala, I. Watts, P. Norreys, and A. Dangor, Phys. Rev. Lett. **85**, 1654 (2000).
[8] A. Maksimchuk, S. Gu, K. Flippo, D. Umstadter, and V. Bychenkov, Phys. Rev. Lett. **84**, 4108 (2000).
[9] A. Snavely, M. Key, S. Hatchett, T. Cowan, M. Roth, T. Phillips, and M. Stoyer, Phys. Rev. Lett. **85**, 2945 (2000).
[10] M. Zepf *et al.*, Phys. Rev. Lett. **90**, 064801 (2003).
[11] M. Hegelish, S. Karsch, G. Pretzler, D. Habs, K. Witte, W. Guenther, M. Allen, and E. A. I. Blazevic, Phys. Rev. Lett. **89**, 085002 (2002).
[12] A. Mackinnon, M. Borghesi, S. Hatchett, M. Key, P. Patel, H.

Campbell, A. Schiavi, R. Snavely, S. Wilks, and O. Willi, Phys. Rev. Lett. **86**, 1769 (2001).
[13] A. Gurevich, L. Pariskaya, and L. Pitaievskii, Sov. Phys. JETP **22**, 449 (1966).
[14] V. Kovalev and V. Bychenkov, Phys. Rev. Lett. **90**, 185004 (2003).
[15] S. Bulanov, N. Naumova, T. Esirkepov, and F. Califano, JETP Lett. **71**, 407 (2000).
[16] Y. Sentoku *et al.*, Phys. Rev. E **62**, 7271 (2000).
[17] M. Passoni, V. Tikhonchuk, M. Lontano, and V. Bychenkov, Phys. Rev. E **69**, 026411 (2004).
[18] S. V. Bulanov, T. Esirkepov, J. Koga, T. Tajima, and D. Farina, Plasma Phys. Rep. **30**, 21 (2004).
[19] Y. Kishimoto, T. Masaki, and T. Tajima, Phys. Plasmas **9**, 589 (2002).
[20] S. V. Bulanov, T. Z. Esirkepov, F. F. Kamenets, Y. Kato, A. V. Kuznetsov, K. Nishihara, F. Pegoraro, T. Tajima, and V. S. Khoroshkov, Plasma Phys. Rep. **28**, 975 (2002).
[21] T. Tajima, *Computational Plasma Physics with Applications to Fusion and Astrophysics* (Addison-Wesley, Reading, MA, 1989).
[22] C. K. Birdsall and A. B. Langdon, *Plasma Physics via Computer Simulation* (McGraw-Hill, New York, 1985).
[23] S. Augst, D. Strickland, D. D. Meyerhofer, S. L. Chin, and J. H. Eberly, Phys. Rev. Lett. **63**, 2212 (1989).
[24] V. A. Vshivkov, N. M. Naumova, F. Pegoraro, and S. V. Bulanov, Phys. Plasmas **5**, 2727 (1998).
[25] T. Z. Esirkepov *et al.*, Phys. Rev. Lett. **89**, 175003 (2002).
[26] L. D. Landau and E. M. Lifshits, *Electrodynamics of Continuous Media* (Pergamon, Oxford, 1988).
[27] F. Brunel, Phys. Rev. Lett. **59**, 52 (1987).
[28] S. V. Bulanov, N. M. Naumova, and F. Pegoraro, Phys. Plasmas **1**, 745 (1994).
[29] J. Dawson, Phys. Rev. **113**, 383 (1959).